Valleriite, a Natural Two-Dimensional Composite: X-ray Absorption, Photoelectron, and Mössbauer Spectroscopy, and Magnetic Characterization

Yuri L. Mikhlin,* Maxim N. Likhatski, Oleg A. Bayukov, Yuriy Knyazev, Dmitriy A. Velikanov, Yevgeny V. Tomashevich, Alexander S. Romanchenko, Sergey A. Vorobyev, Mikhail V. Volochaev, Sergey M. Zharkov, and Debora Motta Meira

Read Online

ACCESS | Metrics & More | Article Recommendations | Supporting Information

ABSTRACT: Valleriite is of interest as a mineral source of basic and precious metals and as an unusual material composed of two-dimensional (2D) Fe–Cu sulfide and magnesium hydroxide layers, whose characteristics are still very poorly understood. Here, the mineral samples of two types with about 50% of valleriites from Noril'sk ore provenance, Russia, were examined using Cu K- and Fe K-edge X-ray absorption fine structure (XAFS) spectroscopy, X-ray photoelectron spectroscopy (XPS), ^{57}Fe Mössbauer spectroscopy, and magnetic measurements. The Cu K X-ray absorption near-edge structures (XANES) spectra resemble those of chalcopyrite, however, with a higher electron density at Cu^+ centers and essentially differ from those of bornite Cu_5FeS_4; the Fe K-edge was less informative because of accompanying oxidized Fe-containing phases. The post-edge XANES and extended XAFS (EXAFS) analysis reveal differences in the bond lengths, e.g., additional metal–metal distances in valleriites as compared with chalcopyrite. The XPS spectra confirmed the Cu^+ and Fe^{3+} state in the sulfide sheets and suggest that they are in electron equilibrium with (Mg, Al) hydroxide layers. Mössbauer spectra measured at room temperature comprise central doublets of paramagnetic Fe^{3+}, which decreased at 78 K and almost disappeared at 4.2 K, producing a series of hyperfine Zeeman sextets due to internal magnetic fields arising in valleriites. Magnetic measurements do not reveal antiferromagnetic transitions known for bornite. The specific structure and properties of valleriite are discussed in particular as a platform for composites of the 2D transition metal sulfide and hydroxide (mono)layers stacked by the electrical charges, promising for a variety of applications.
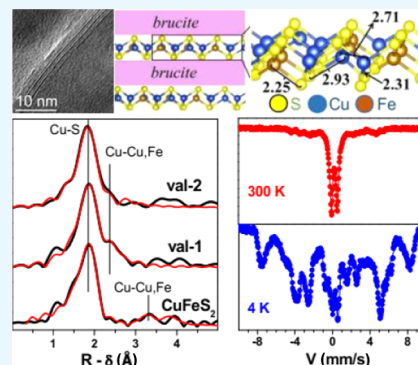
INTRODUCTION

Valleriite is a mineral with an unusual structure formed by alternating quasi-monolayers of brucite-type $yMg(OH)_2 \cdot zAl(OH)_3$ and sulfide monolayers close to $CuFeS_2$.[1–11] Found in many locations since 1960s, valleriite is not abundant and, generally, has limited commercial importance. At the same time, so-called "coppery" ores of Noril'sk ore provenance in Russia (5–8% of total deposits) contain up to 20% of valleriite, industrial values of copper, nickel, and platinum group metals.[12–14] Valleriite is densely overgrown with serpentines, pyrrhotite, chalcopyrite, aluminosilicates, etc., and the beneficiation of valleriite-containing ores using froth flotation and other separation techniques is poor due to special and scarcely understood properties of valleriite and a depressing effect of serpentines. Direct extraction of metals and chemical conversion of valleriite to simple sulfide phases have been suggested but not implemented in any technologies (see ref 14 and references therein). On the other hand, low-dimensional materials, such as graphene, van der Waals crystals, MAX and MXenes, transition metal dichalcogenides, and ternary

chalcogenides,[15–24] attract huge attention owing to their unique physical properties, including magnetic, and much efforts are being taken to discover new two-dimensional (2D) materials nowadays. Naturally occurring minerals like valleriite, which is composed of "noncommensurate" sulfide and hydroxide quasimonolayers[1] with very diverse chemical, electronic and magnetic characters, may offer some clues as promising prototypes of the novel (nano)composite materials (see, for example, refs 24–26).
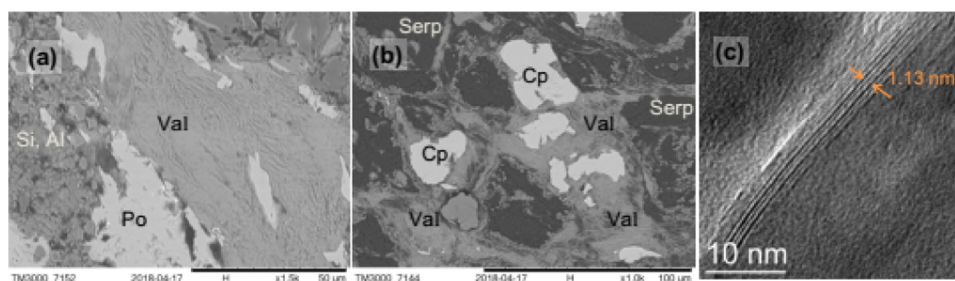
The composition of valleriites depends on their origin.[11,27–30] The brucite-like layers, which are believed to contain some Fe^{2+}/Fe^{3+} ions substituting Mg^{2+} and Al^{3+} cations in octahedral coordination to OH^- anions, can be
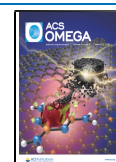
Figure 1. SEMs of samples' polished sections of (a) valleriite-1 and (b) valleriite-2 (Val: valleriite, Si, Al: Mg- and Al-bearing silicates, Po: pyrrhotite, Cp: chalcopyrite, Serp: serpentines), and (c) TEM image of the valleriite nanocrystal.

described as $m[\mathrm{Mg, Fe}](\mathrm{OH})_2] + n(\mathrm{Al, Fe})(\mathrm{OH})_3$, where $1.3 \leq m \leq 1.6$ and $0 \leq n \leq 0.3$.[2,3,11,14,28−30] The sulfide part $\mathrm{Cu}_x\mathrm{Fe}_y\mathrm{S}_2$ usually has x and y within the range 1 ± 0.3 or narrower; in particular, Hughes et al.[3] have found that synthetic valleriites were stable in the range from $[\mathrm{CuFeS}_2]\cdot 1.67[\mathrm{Mg}_{0.70}\mathrm{Al}_{0.30}(\mathrm{OH})_2]$ to $[\mathrm{Cu}_{1.30}\mathrm{Fe}_{0.70}\mathrm{S}_2]\cdot 1.35\text{-}[\mathrm{Mg}_{0.74}\mathrm{Al}_{0.26}(\mathrm{OH})_2]$. X-ray diffraction (XRD) studies[1] have confirmed that the sulfide sublattice is rhombohedral (space group $R\bar{3}m$) with hexagonal axes $a = 0.3792$ nm and $c = 0.341$ nm; the hydroxide layers have hexagonal lattice (space group $P\bar{3}m1$) with $a = 0.307$ nm and $c = 1.137$ nm. Cu and Fe atoms are considered randomly occupying all of the tetrahedral sites within a pair of close-packed atomic S layers. The hydroxide layers are believed to bear a positive electric charge caused by the substitution of Mg^{2+} with Al^{3+}; correspondingly, the sulfide layers are charged negatively. The layers have been found to be partially mismatched in both natural and synthetic valleriite samples.[5] X-ray photoelectron spectroscopy (XPS) studies[3,30,31] suggest that the nominal oxidation states of metals in the sulfide layers seem to be Cu^+ and Fe^{3+}, similar to chalcopyrite. However, antiferromagnetic ordering is absent; room-temperature $^{57}\mathrm{Fe}$ Mössbauer spectroscopy studies have found paramagnetic signals from a series of $\mathrm{Fe}^{3+}/\mathrm{Fe}^{2+}$ centers preferentially coordinated with S but occurring also in the brucite-like layers, along with chalcopyrite, magnetite, and other impurities both in natural and synthetic samples.[5,10,30,32−34]

The complex composition of natural samples makes the separation of pure valleriite and exploration of its electronic structure, chemical and physical characteristics difficult. Thermal or hydrothermal syntheses of valleriite also have yielded less than 50% of valleriite mixed with metal (hydro)oxides and sulfides.[3,29,32−34] In the current research, we performed the element-specific X-ray absorption fine structure (XAFS) spectroscopy of the Cu K- and Fe K-edges, XPS, and $^{57}\mathrm{Fe}$ Mössbauer spectroscopy in conjunction with magnetic susceptibility measurements at room and cryogenic temperatures in order to elucidate the structure of valleriites in two types of mineral assemblages from the Noril'sk ore deposit. The mineral samples were thoroughly characterized using mineralogical analysis, electron microscopy, and related analytical techniques (energy dispersive X-ray (EDX), elemental mapping), XRD, transmission electron microscopy (TEM), and so on. This approach allowed to reveal, particularly, a set of magnetic hyperfine interactions involving Fe centers in the sulfide layers at reduced temperatures, which depict valleriite as a new 2D material with, among others, interesting magnetic properties. The results are also important for understanding the origin and behavior of valleriite in nature and mineral processing.

EXPERIMENTAL SECTION

Materials. Natural valleriites from two locations of the Talnakh deposit (Noril'sk ore field, Russia) were used in the experiments. Valleriite of the first type (valleriite-1) is mainly represented by grains associated with pyrrhotite (preferentially hexagonal $\mathrm{Fe}_9\mathrm{S}_{10}$), silicates, and aluminosilicates. The second type of mineral samples (valleriite-2) is composed of valleriite veins in Mg-bearing serpentines (lizardite and others) and chalcopyrite CuFeS_2. Figure 1 shows scanning electron micrographs (SEMs) of the sample sections and an example of a high-resolution TEM image of a layered valleriite nanocrystal. Additional microscopic images, EDX, elemental mapping, XRD, and other data can be found in the Supporting Information. The typical composition of valleriite-1 determined using EDX analysis is (atom %): O 52.0, S 20.3, Mg 14.9, Fe 8.8, Cu 4.1, Al 2.0, Ca 0.72; and the composition of valleriite-2 is (atom %): O 47.9, S 17.2, Mg 13.7, Fe 8.0, Cu 7.5, Al 4.6, Si 0.51, Ca 0.50. The first type is characterized by enhanced concentrations of sulfur and iron, which may be partially due to pyrrhotite and ultrafine particles adhered to the valleriite surface upon polishing the cross-sections. The composition of the sulfide part of valleriite-2 is close to CuFeS_2 with almost equal amounts of Cu and Fe. So, the samples of valleriite-1 have a negligible content of chalcopyrite, and Cu occurs only in valleriite, while the valleriite-2 samples contained comparable quantities of valleriite and chalcopyrite and very minor amounts of Fe and Cu in other phases. Some additional characteristics, including soft XANES, of analogous samples were published in refs 14, 31, 35 Chalcopyrite CuFeS_2 from Primorsky (Russia) and synthetic low-temperature bornite $\mathrm{Cu}_5\mathrm{FeS}_4$ used as reference materials were described in detail elsewhere.[36−38]

For Mössbauer spectroscopy and XRD, the minerals were ground in an agate mortar to a particle size of about 50 μm; SEM, XAFS, and XPS experiments were performed both with the ground specimens and mineral lumps of a few millimeters in size, and obtained essentially the same results.

All measurements were repeated with at least two different specimens both of valleriite-1 and valleriite-2 in order to ensure that the results are representative and effects of occasional mineral impurities are insignificant (or can be evaluated).

CHARACTERIZATION

Electron Microscopy and X-ray Diffraction. The samples were embedded in epoxy resin, polished, and characterized using scanning electron microscopy (SEM), backscattered electron imaging microanalysis (SEM−BSE), and energy-dispersive X-ray analysis (EDX) utilizing a Hitachi TM 3000 instrument operated at an acceleration voltage of 15

kV, equipped with a Bruker Quantax 70 EDX analyzer. Transmission electron microscopy (TEM) images, EDX, and selected area electron diffraction patterns (SAED) were acquired from ground samples using a JEM-2100 instrument (JEOL) operated at 200 kV. For the TEM experiment, the particles were dispersed in ethanol, and then a droplet of the suspension was placed on a carbon-coated copper grid and allowed to dry at room temperature. X-ray powder diffraction patterns were recorded using a PANalytical X'Pert Pro diffractometer with Cu Kα radiation.

X-ray Absorption Spectroscopy. Cu K-edge and Fe K-edge X-ray absorption near-edge structures (XANES) and extended X-ray fine structures (EXAFS) were measured at the bending magnet beamline BM23 (European Synchrotron Radiation Facility, Grenoble, France) at room temperature in the fluorescence mode using a Vortex silicon drift X-ray detector. The storage ring operated in the 16-bunch mode with an average current of 90 mA. X-ray irradiation was monochromatized with a double-crystal Si(111) monochromator and an Rh mirror to reject the harmonics;[39] the size of the beam at a sample was 0.1×0.3 mm^2. The monochromator was calibrated to the first maximum in the first derivative of the Cu K-edge absorption spectrum of a metallic copper foil and the Fe K-edge spectrum of an iron foil, respectively, which were continuously collected in the transmission mode during sample measurements. The EXAFS data were collected up to 15 Å^{-1}, with a variable sampling step in energy (5 eV in the pre-edge region, 0.5 eV in the XANES region, and Δk constant in the EXAFS region with 0.03 Å^{-1} step), and an integration time of 3 s. Typically, 2−3 specimens of each mineral were examined, and 2−3 scans were averaged for each spectrum. Both Cu K- and Fe K-edge XAFS spectra were treated applying standard procedures implemented in the Demeter software package (version 0.9.26) based on the IFEFFIT program, version 1.2.12.[40] The k^2-weighted Cu K-EXAFS oscillations were processed with the photoelectron wavevector k in the range 2.3−11.5 Å^{-1}, using a Hanning window with a sill width of 3 Å^{-1}. The Fourier transformed R-space data were windowed in the range of 1.0−2.314 and 3.082 Å for valleriites and chalcopyrite, respectively. The photoelectron threshold energy E_o was first fitted from the data and then kept constant. The EXAFS signals were simulated utilizing a single-path scattering approach.

X-ray Photoelectron Spectroscopy. The photoelectron spectra presented here were recorded with a SPECS spectrometer equipped with a PHOIBOS 150 MCD9 hemispherical energy analyzer using Mg Kα radiation of the dual anode X-ray tube at an analyzer transmission energy of 20 eV for the survey spectra or 8 eV for narrow scans. The binding energies were calibrated against the C 1s line of the adventitious carbon (285.0 eV); a low-energy electron source FG 20 (SPECS), applied to eliminate heterogeneous electrostatic charging, was operated with an electron energy of 0.05 eV and a current of 10 μA. The spectra were fitted after subtraction of the Shirley-type nonlinear background using the Gauss−Lorentz peak shape using the CasaXPS software package.

Mössbauer Spectroscopy. Transmission Mössbauer experiments were carried out using an MC-1104Em spectrometer with a ^{57}Co(Rh) source; the source was kept at room temperature, while the absorber was either at the ambient temperature or cooled down to liquid nitrogen (78 K) and liquid helium (4.2 K) temperatures. The powder samples

(about 3 mg/cm^2 of Fe in thickness) sealed with Kapton tape were attached to an Al sample holder. Isomer shifts (IS) are given relative to α-iron at room temperature. Probabilities P of the quadrupole splitting $P(QS)$ for doublets and of magnetic hyperfine fields $P(H)$ for sextets were first determined from the experimental spectra. In the second stage, these data were used to generate a model spectrum and then to fit the experimental spectra varying the full set of parameters.[41,42]

Magnetic Measurements. The magnetization of valleriite samples was measured utilizing a superconducting quantum interference device (SQUID) magnetometer[43] with a magnetic field H of 500 Oe (field-cooled [FC] and zero-field-cooled [ZFC], respectively) as the temperature varied from 4.2 to 290 K. The magnetic moment was also determined as a function of the magnetic field H in the range from −800 to 800 Oe at several temperatures. Magnetization in stronger fields was examined using a vibrating sample magnetometer with a Puzey electromagnet[44] in the temperature range of 78−300 K.

RESULTS AND DISCUSSION

X-ray Absorption Spectroscopy. The Fe K- and Cu K-edge XANES spectra from valleriites are compared with the spectra of chalcopyrite (CuFeS$_2$) and bornite (Cu$_5$FeS$_4$) in Figure 2. The Fe K near-edge structures are distinct for the two
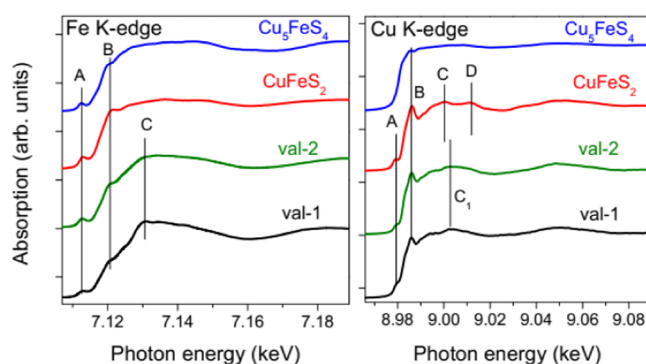

Figure 2. Fe K-edge and Cu K-edge XANES spectra of two valleriites: chalcopyrite (CuFeS$_2$) and bornite (Cu$_5$FeS$_4$).

valleriites due to various contents of iron- and oxygen-bearing substances. The main features in the spectra are the pre-edge peak A originating from electronic transitions from the core Fe 1s to vacant 3d states mixed with Fe 4p and S 3p or O 2p states, the white line B (∼7121 eV) attributed to the transitions to Fe 4p states hybridized with sulfur states in the sulfide phases, and the maxima C near 7130 eV from Fe atoms bonded to oxygen in oxide, including the products of oxidation of pyrrhotite and other sulfides, and silicate phases.[45−48] The Fe K-XANES spectra of valleriites seem to be closer to that of bornite than chalcopyrite;[49−52] we, however, refrain from further discussion of these spectra because of the multiphase composition of the samples.

The Cu K-edge X-ray absorption spectra are more informative since valleriite is the only Cu-bearing phase in valleriite-1, and sample-2 contains comparable quantities of valleriite and chalcopyrite. The Cu K-edge XANES spectra of both valleriites resemble that of chalcopyrite with Cu$^+$ in tetrahedral coordination with sulfide ions,[49−52] but not low bornite whose crystalline lattice consists of sphalerite-type and antifluorite-type subcells.[53,54] The pre-edge peak A corresponds to transitions from Cu 1s to empty states having Cu 3d

character (despite the Cu 3d band being nominally full), which are forbidden by dipole selection rules but emerged in the spectra due to 3d + 4p mixing and quadrupole coupling.[49−52] In valleriites, feature A is widened and shifted to higher energy, similar to the spectrum of bornite, and the intensity of peak B at 8986.0 eV from 1s to 4p transition decreases in comparison with chalcopyrite. The changes in the position and intensity of the features can be interpreted in terms of disordering and a decrease of coordination number of Cu atoms and/or lowering the positive charge at Cu atoms relative to $CuFeS_2$. This concurs with the decrease of the leading peak at Cu L_3-edge at 932.6 eV[31] attributed to Cu 2p → 3d transitions that indicates a smaller number of holes in the formally Cu d^{10} band in valleriite than in chalcopyrite. In addition, post-edge maximum C blue-shifted and maximum D disappeared in valleriites. The features are believed to be shape resonances caused by multiple electron scattering,[49,55] which have been assigned to interatomic distances of 3.74 Å (Cu−Cu, Fe) and 2.64 Å (interplanar length d_{200}), respectively, for chalcopyrite.[55] It is anticipated that the crystalline lattice distances and some bonds of chalcopyrite disappeared in valleriite, and the spectrum of valleriite-2 should be an intermediate between valleriite-1 and chalcopyrite, while the post-edge features are very close to valleriite-1. We may suggest that this is due to alterations of the reacting chalcopyrite, as will be discussed below.

The Cu K-edge EXAFS results obtained for valleriites are presented in Figure 3a,b and Table S1 (Supporting
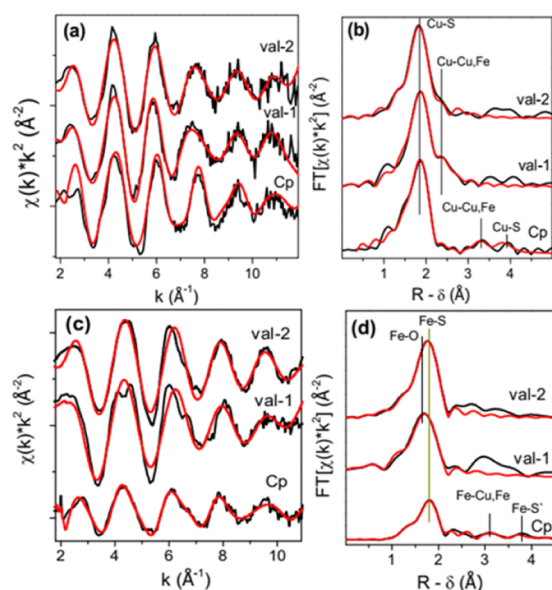
Figure 3. (a, b) Cu K- and (c), (d) Fe K-edge EXAFS data for chalcopyrite (Cp) and the samples of valleriite-1 and 2 (val-1 and val-2): (a), (c) the k^2-weighted experimental data (black lines) and the corresponding fit (red lines); (b), (d) Fourier transform magnitudes of these data and their fits in R-space (without phase corrections).

Information) in comparison with chalcopyrite. The clear differences in the experimental data between the minerals are observed in the k range from 7 to 8 Å^{-1}. The model taking into account the two coordination shells of a central copper atom gives good fits of this and other features, while application of the three-shell model that includes longer Cu−S bonds does not improve the fitting. The simulation (Table S1) revealed Cu−S distances of 2.28−2.31 Å and a number N_S of 3.4 for the

nearest S neighbors for both valleriites as compared with the values of 2.28 Å and 3.8, respectively, for chalcopyrite. The values are in reasonable agreement with the coordination numbers and interatomic distances derived from X-ray diffraction; particularly, Evans et al.[1] have found one apical (Fe, Cu)−S bond of 2.41 Å and three basal bonds of 2.30 Å for valleriite. Also, EXAFS revealed a Cu−(Cu, Fe) bond length of 2.71 Å, which is absent in chalcopyrite but corroborates the (Fe, Cu)−(Fe, Cu) distance of 2.77 Å reported in ref 1. The bonds are also in agreement with those derived from the shape resonance positions in Cu K-XANES (Figure 2). A scheme illustrating the structure and bond lengths in sulfide layers of valleriite in comparison with chalcopyrite is given in Figure 4.
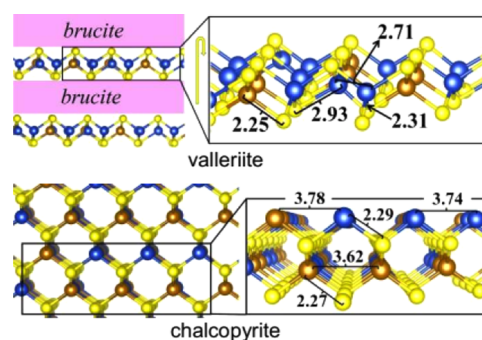
Figure 4. Fragments of a structure of valleriite in the crystallographic direction (120) and a lattice of chalcopyrite in the direction (021), and interatomic distances (Å) as determined from EXAFS. Right-hand panels show the sulfide fragments enlarged and slightly turned for clarity. S atoms are yellow, Cu atoms are blue and Fe atoms are brown. The ordered occupancy of Cu and Fe centers is conventionally shown in valleriite.

Figure 3c,d and Table S2 show the Fe K-edge EXAFS of valleriites and chalcopyrite. The substantially reduced numbers of neighboring S atoms are indicative of both Fe−S and some Fe−O bonding, especially in the case of valleriite-1 owing to oxidized pyrrhotite. The Fe−S distances are slightly shorter than those in chalcopyrite and the Cu−S ones in valleriite but, again, the Fe K-edge data are inconclusive because of the complex composition of the samples. It is noteworthy that Cu and Fe atoms have been suggested[1] to be statistically distributed in cationic positions of the sulfide structure of valleriite, in contrast to chalcopyrite; unfortunately, EXAFS fails to confirm any clustering of the metal atoms due to similar scattering of Cu and Fe.

X-ray Photoelectron Spectroscopy. The surface concentrations of elements derived from the XPS survey spectra (Figure 5) approximately agree with the compositions determined using EDX analysis and hard X-ray photoelectron spectroscopy (HAXPES) reported previously.[31] It is noteworthy that the contents of Mg, Al, and Si are notably higher than those of Cu, Fe, and S because ultrafine particles of aluminosilicates and especially serpentines tend to attach to the surfaces of valleriite and metal sulfides.[35] The high-resolution photoelectron spectra were collected from the ground valleriite samples with and without low-energy electron flooding in order to eliminate (inhomogeneous) electrostatic charging. The relative intensities of the components shifted to higher BEs owing to the charging without the flood gun applied were large for O, C, and Si spectra, less significant for Fe, Mg, and Al, and minimal for S and Cu. The findings
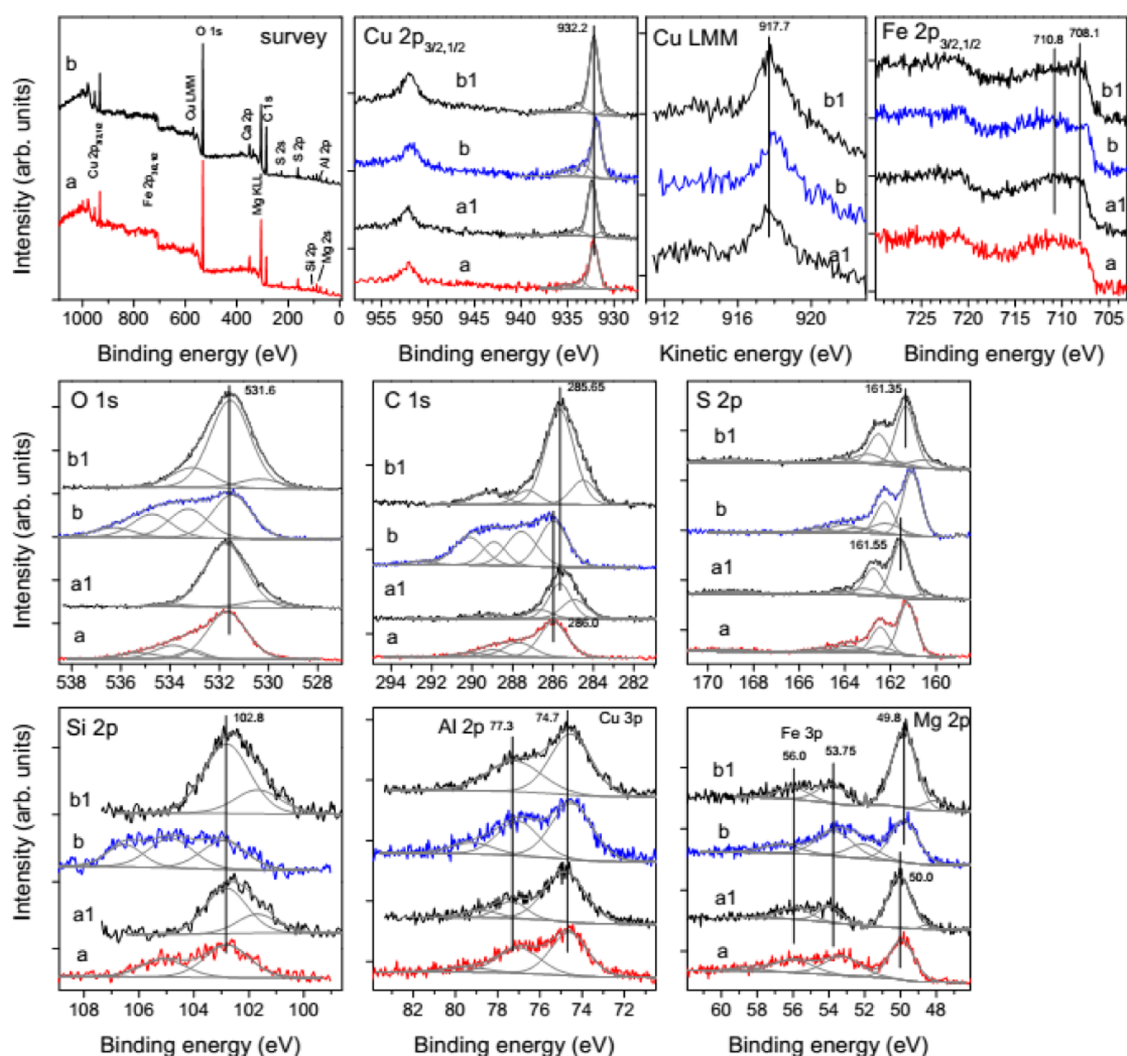
Figure 5. X-ray photoelectron spectra of valleriite-1 (a, a1) and valleriite-2 (b, b1) without (a, b) and with (a1, b1) slow electron flooding.

suggest the same small charging of 0.1−0.2 eV for the sulfide and brucite-like hydroxide layers, in contrast to iron oxy-hydroxides, silicates, and other gangue minerals.

The quite narrow spectra of copper with the major Cu 2p$_{3/2}$ peak at 932.2 ± 0.1 eV are characteristic of Cu$^+$ bonded to S;[37,38,56] Cu^{2+} species are negligible as the shake-up satellites in the spectral region of 940−944 eV are very weak if any. The Cu L$_3$MM Auger peak is located at a kinetic energy of 917.6 ± 0.1 eV for both samples. This concurs with the spectra of sulfur with the major peak S 2p$_{3/2}$ at 161.5 eV for valleriite-1 and 161.35 eV for valleriite-2, typical for monosulfide, along with minor di- (∼162.5 eV), polysulfide (∼163.6 eV), and sulfate (169 eV) signals, which arise upon surface oxidation of metal sulfides, including pyrrhotite and chalcopyrite.[38] The Fe 2p spectra comprise contributions from both Fe^{3+}−S (Fe 2p$_{3/2}$ at about 708.0 eV), likely Fe^{2+}−S (e.g., in pyrrhotite) and Fe^{3+}−O species (BEs of 710 eV and higher). The latter exhibited a notable shift due to the electrostatic charging and can be largely related to admixture phases rather than Fe in hydroxide layers of valleriite. Fitting the Fe 2p spectra composed of several chemical species with their multiplet structures[57] is not reliable and omitted here.

The results are in reasonable agreement with the X-ray absorption spectra (Figures 2 and 3) and the photoelectron spectra reported previously,[3,4,31] although the earlier data are sometimes contradictory. For example, Li and Cui[4] have reported the energies uncorrected for electrostatic charging, incomparable with those from other studies. The S 2p spectra of two synthetic samples studied by Hughes and co-workers[3] were different, probably, because of essentially oxidized sulfide surfaces. Nonetheless, all of the XPS data are clearly indicative of Cu$^+$, suggesting therefore predominant Fe^{3+} state in the sulfide sheets of valleriites.

Mössbauer Spectroscopy. ^{57}Fe Mössbauer spectra of the two valleriite samples are shown in Figure 6, and the fitting parameters are summarized in Tables S3 and S4; the probabilities of quadrupole splitting P(QS) for doublets and of internal hyperfine fields P(H) for sextets determined in the experimental spectra are presented in Figure S4 (Supporting Information). The room-temperature spectra of both samples are dominated by a central signal, whose relative intensities (60−75%) correlate with the share of iron in valleriites derived from XAFS, XRD, and EDX. The spectrum of valleriite-1 is fitted with a major doublet d1 with the isomer shift (IS) of 0.38 mm/s and QS of 0.64 mm/s, which is attributed to paramagnetic Fe^{3+} in tetrahedral coordination with S in the sulfide sheets of valleriite, in accordance with the previous studies,[5,10,30,32−34] and three six-line Zeeman components with
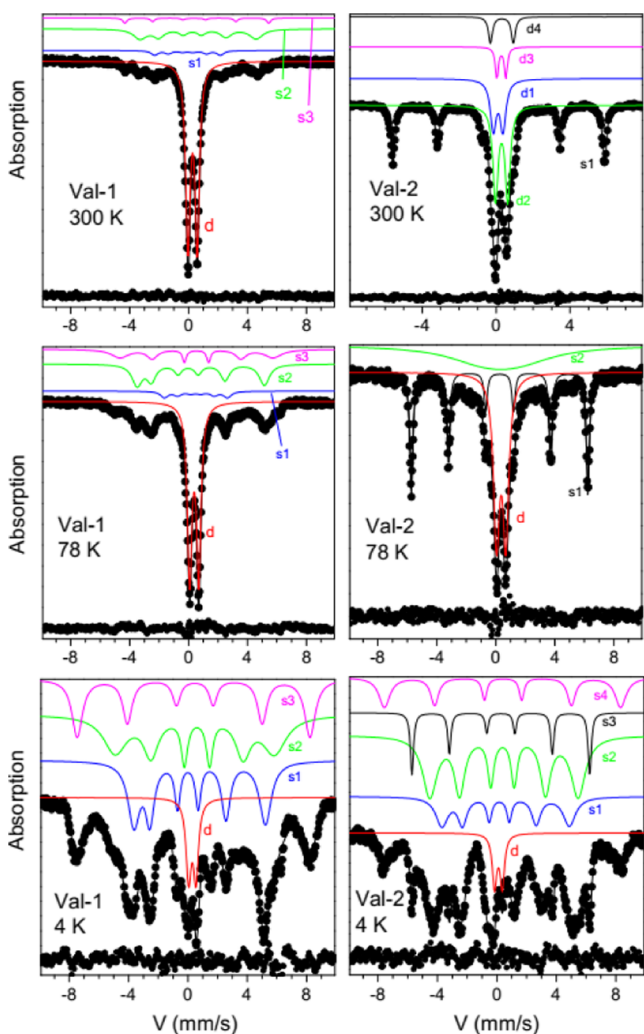
Figure 6. ^{57}Fe Mössbauer absorption spectra (dots) of valleriite-1 (Val-1) and valleriite-2 (Val-2) samples measured at different temperatures and the results of fitting (color lines) summarized in Tables S3 and S4 (Supporting Information); smaller dots are differences between experimental spectra and fits.

the isomeric shift (IS) of 0.66 mm/s and hyperfine fields (H) of 223-201 (Table S3) attributable to high-spin Fe^{2+} atoms in pyrrhotite $Fe_{1-x}S$.[58−64]

The room-temperature spectrum of the second sample (Figure 6) is composed of a sextet with an isomeric shift of 0.25 mm/s and hyperfine field of 355 kOe (QS ~0 mm/s) from Fe^{3+} in chalcopyrite,[32,54,64−67] and the central signal that is notably broader than that of valleriite-1 and is better fitted with four doublets. One of them with IS = 0.22 mm/s appears to belong to Fe^{3+} bonded with oxygen in hydroxide layers,[30] and three others with IS ~0.4 and QS = 0.49−1.24 mm/s are due to Fe^{3+} centers coordinated to 4 S atoms with varying distortion of the local environment (Table S4). The fit and its interpretation is close to that proposed by Waanders and Pollak[30] although they have assigned the smaller doublet with an IS of ~0.4 and QS of 1.12−1.32 mm/s to high-spin Fe^{2+}-S species. The rationalization of Mössbauer parameters of synthetic and natural samples by Qin et al.[5] and Chistyakova and co-workers[32−34] was principally similar. The parameters of main paramagnetic doublets are consistent with Fe^{3+} bonded with sulfide anions akin to bornite Cu_5FeS_4 and cubanite

$CuFe_2S_3$,[54] despite a higher quadrupole splitting (~0.6 vs 0.22 mm/s in bornite) probably owing to the essentially distorted Fe−S coordination (Figure 3). So, the Mössbauer paramagnetic signal is due to predominant Fe^{3+}−S centers along with smaller contributions of other species, e.g., iron coordinated with hydroxide anions in brucite-like layers of valleriites.

The central doublets of both valleriites shift to a higher IS (~0.5 mm/s) as the temperature decreased to 78 K and their intensities decrease, especially at 4.2 K, while the lines of hyperfine magnetic structure emerge, or drastically increase, indicating ordering of Fe spins. For valleriite-1, the sextets of pyrrhotite probably incorporate some responses from valleriite at 78 K. When the temperature drops to 4.2 K, the spectrum of pyrrhotite can be approximated by one sextet s2 (IS = 0.65 mm/s and H = 333 kOe) with wide lines and a population of about 36% (Table S3) as a result of the phase transition at 32 K.[60,68−71] Two other sextets s1 and s3 that arise from the doublet of valleriite-1 reflect different distortions of the local environment (QS = 1.6 and −0.16 mm/s) and distinct magnetic interactions (H = 275 and 487 kOe) (Table S3) at iron sites in the valleriite layers.

The spectrum of valleriite-2 measured at 4.2 K also consists of a series of Zeeman sextets, with one of them (s3) clearly originating from chalcopyrite. The sextets s1 and s4 resemble those in valleriite-1, though somewhat differing in parameters and intensities (Table S4). The sextet s2 (IS = 0.54 mm/s, QS = 0.2 mm/s, and H = 310 kOe) can arise from valleriite too, taking in mind the complex nature of the broad doublet at RT. Alternatively, this feature may arise from chalcopyrite as the sextet s3 intensity is almost three times less than that at higher temperatures (Figure 6, Table S4). Since no significant changes in the spectra of chalcopyrite at low temperatures have been reported in the literature,[53,54,72,73] we may suggest that Fe^{3+} centers both in defective chalcopyrite (possibly, an intermediate product of its reaction with serpentine) and valleriite contribute to the sextet s3. The spectra of both samples measured at 4.2 K contain weak paramagnetic doublets with the Mössbauer parameters attributable both to sulfide and oxide local environment of Fe.

Although the accurate assignment of the hyperfine magnetic sextets, as well as the "residual" doublets, remains challenging, they definitely arise at the expense of the room-temperature paramagnetic signal of valleriite. A similar effect of temperature is well-known for bornite, in which the IS of the central doublet increases from 0.38 mm/s at room temperature to ~0.5 mm/s at 70 K due to the second-order Doppler shift, and the QS almost does not change; that is typical for high-spin Fe^{3+}.[54] The hyperfine structure arises in bornite at 65 K as three sextets with H of about 200 kOe and evolved at lower temperatures to a single six-line pattern with IS = 0.53 mm/s, QS ~ 0, and H = 352 kOe. The Mössbauer spectra of valleriite having similar IS and H parameters agree with mainly Fe^{3+} in the sulfide layers but QS is larger because of the lower coordination symmetry. The compositional and structural disorder in valleriites causes the appearance of several low-temperature hyperfine patterns.

Magnetic Properties. Figure 7 shows the temperature dependences of magnetization of valleriite samples and the hysteresis loop for valleriite-1 at 4.2 K. The magnetization of valleriite-2 is rather simple, exhibiting a linear dependency of magnetization vs field H, which is due to the antiferromagnetic phase of chalcopyrite[54,72−74] and paramagnetic character of
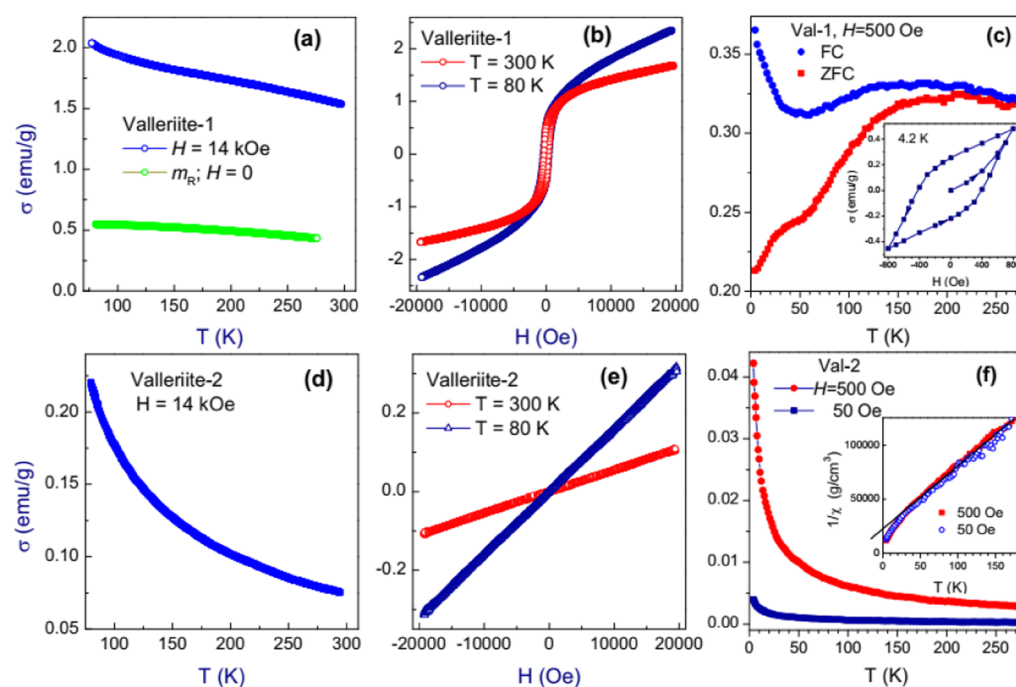
Figure 7. Temperature (a, c, d, f) and field (b, e) dependences of magnetization of (a−c) valleriite-1 and (d−f) valleriite-2. Plots (c) and (f) are measured using a SQUID in magnetic fields of 500 Oe and a ZFC mode along with magnetic hysteresis loop at 4.2 K (insertion) for valleriite-1 (c), and in the fields of 500 and 50 Oe for valleriite-2 (f) (inset: reciprocal susceptibility χ vs temperature plots).

valleriite. The plots of reciprocal magnetic susceptibility χ versus temperature are linear until about 30 K, and the slope increases at lower temperatures (Figure 7f) due to a contribution of antiferromagnetic chalcopyrite.[53,54,73−75]

The magnetization of valleriite-1 can be described as a sum of ferromagnetic, antiferromagnetic, and paramagnetic components, which are often difficult to separate in complex mineral systems.[75,76] A minor amount of ferromagnetic phase (e.g., monoclinic pyrrhotite), magnetite Fe_3O_4, and/or some others seem to be responsible for the hysteresis loop.[76,77] Both pyrrhotite and magnetite have the phase transition nearby 130 K.[68−71,76,77] Magnetization below 30 K can be related to a growing paramagnetic component; the effect is observable in the strong field of 14 kOe starting from ∼150 K. On the other hand, such a behavior may be due to short-range antiferromagnetic interactions.[24] No clear signs of superparamagnetic blocking and (super)spin-glass freezing in valleriite, which are typical for magnetic nanoparticles and nanolayered structures, for example,[78−81] were found. At any cost, no paramagnetic-to-antiferromagnetic state transitions were observed in both valleriites, in contrast to bornite with a Néel temperature of 65 K.[53,54,82,83]

Chemical Bonding in Sulfide Sheets and Implications for the Formation of Valleriite. The combination of element-sensitive Cu K- and Fe K-edge X-ray absorption spectroscopy together with previous soft XANES studies (Cu L-, Fe L- and others),[31] XPS, and Mössbauer spectroscopy allow us to shed new light onto the chemical states of copper and iron. All of the methods support the main oxidation states as Cu^+ and Fe^{3+}, despite some uncertainty in the interpretation of Mössbauer spectra. The Cu K-edge absorption spectra demonstrate that valleriites are closer to chalcopyrite than bornite Cu_5FeS_4. However, the local positive charges at Cu and probably Fe sites in the sulfide layers are lower while the electron density at S atoms is insignificantly higher than in

chalcopyrite. This may be explained in terms of either specific chemical bonding in the two-dimensional structures or negative charging of the layers stacked between the hydroxide layers bearing a positive charge.[1] It is noteworthy that the electrostatic charging of both layers is equal and low under the XPS experiment conditions, implying a kind of electronic equilibrium in the nanocomposite and delocalization of electrons over the sulfide sheets.

There are some compositional and structural differences between valleriite-1 and valleriite-2. The first valleriite sample is not associated with chalcopyrite and contains a higher amount of Fe and lower amounts of Cu and Al. The additional iron is mainly associated with pyrrhotite (Figures 1, S2) but one can expect that the phase interactions under geological conditions result in substitution of some Cu and Al (Mg) by Fe both in sulfide and brucite-like layers of valleriite. Nevertheless, Mössbauer spectra indicate that the Fe positions in valleriite-1 are more ordered. Valleriite in sample-2 closely intergrown with $CuFeS_2$ and serpentine is the product of an incomplete reaction between these minerals. Some signs, particularly Cu K post-edge features almost identical for valleriite-1 and valleriite-2 and tentative splitting of the Mössbauer signal of chalcopyrite in valleriite-2 at 4.2 K, infer certain changes of intrinsic chalcopyrite during the reaction. For example, the near-surface regions of the "reacted" chalcopyrite can have partially disordered or/and nanoparticulate structures.[35−37,84−86] These mechanisms, which are important for understanding the formation of such unusual 2D composites and the mineral processing performance, require further investigation.

Magnetism in Valleriites. Mössbauer spectra of valleriites exposing Zeeman splitting due to internal magnetic fields at low temperatures were compared with that of bornite, Cu_5FeS_4. Meanwhile, the nature of the high-temperature disorder (caused by a partial disordering of the Fe^{3+} and Cu^+ in

the considered sites, or a partial charge transfer between Fe^{3+} and Cu^+) and the paramagnetic-to-antiferromagnetic transition at 65 K, which can be ascribed either to a structural transformation (the reduction of lattice symmetry) or electron spin ordering in bornite, are still disputable.[53,54,82] The hyperfine magnetic interactions are more nontrivial in valleriites as occurring in the two-dimensional Fe–Cu sulfide sheets and, possibly, dielectric (Mg, Al, Fe) hydroxide quasi-monolayers coupled by the opposite electric charges. The similarity between valleriite-1 and valleriite-2 means that the effects do take place in the composites but not in impurity phases, and the multiplicity of the hyperfine sextets implies several distinct spin-ordering patterns, comparable but not identical in the two valleriites. In contrast to chalcopyrite and bornite, valleriites did not show antiferromagnetic character. Magnetic effects in valleriites can be modified via a number of factors, for example, compositions of sulfide (Fe, Cu)S_2 and hydroxide (Mg, Al, Fe)(OH)$_{2+x}$ layers and their electrical charges, a number of the atomic layers, external electric and magnetic fields, and so on. Moreover, the composition of valleriite-like materials can be changed in a very wide range as there exist minerals in which magnesium is replaced by iron in hydroxide layers ("ferrovalleriite"),[27,87] or iron is substituted by chromium in sulfide sheets,[88,89] or mackinawite-type iron sulfide layers with no copper in tochilinite or ferrotochilin-ite.[32,33,90−92] In addition to the magnetic properties, super-conductivity has been reported in such iron chalcogenide layers.[24] Consequently, valleriite emerges as a platform for numerous two-dimensional composite materials, exhibiting very special and tunable properties for various applications. Further studies should be focused on the preparation and characterization of pure synthetic analogues with well-controlled composition and structure, as well as on detailed examination of natural samples.

CONCLUSIONS

Two mineral assemblies from Noril'sk ore deposition containing about 50% of valleriite composed of stacked 2D sulfide (Cu, Fe)S_2 and brucite-like (Mg, Al, Fe)(OH)$_2$ quasi-monolayers were examined. The first valleriite was associated mainly with pyrrhotite Fe_9S_{10}. The second one accompanied by chalcopyrite and serpentine was the product of the incomplete reaction between them. The X-ray Cu K-edge absorption spectra (XANES and EXAFS) collected in the fluorescence mode are close for both valleriites and somewhat different from chalcopyrite, showing a less positive charge localized at Cu^+ centers and additional Cu-(Cu, Fe) distances of about 2.7 Å, while some other bonds did not manifest themselves in EXAFS and in XANES (as post-edge shape resonances). These findings agree with the crystal structure of valleriites and possibly hint at some changes occurring in the near-surface layers of chalcopyrite as intermediate of the reaction. The Fe K-edge XAFS showed significant contributions of surface products of oxidation of sulfides and was insufficiently informative in terms of chemical bonding in valleriites. The XPS data confirmed the Cu^+ and Fe^{3+} state in the sulfide part of valleriites and suggested that the sulfide and (Mg, Al) hydroxide layers are in a sort of electron equilibrium. It was discovered by ^{57}Fe Mössbauer spectroscopy that the central signals attributed to paramagnetic Fe^{3+} in valleriites and dominated the spectra at room temperature decrease at 78 K and almost disappear at 4.2 K. Instead, a series of Zeeman sextets similar but not identical for valleriite-1 and valleriite-2

arise, indicating internal hyperfine magnetic fields in the 2D layers. Magnetic measurements revealed the paramagnetic behavior of valleriites to be different for the two samples but antiferromagnetic transitions, which can be expected by analogy with bornite and chalcopyrite, are absent. The unusual structure and properties of valleriite that can be widely tuned via its composition and other parameters, including the electric charge of the layers, make it a promising prototype for a family of composites of transition metal sulfide and hydroxide (mono)layers. The new insights are also important for understanding the formation and processing of valleriite-containing ores.

ASSOCIATED CONTENT

ⓈⒾ Supporting Information

The Supporting Information is available free of charge at https://pubs.acs.org/doi/10.1021/acsomega.0c06052.

> SEM, EDX, element mapping (Figures S1, S2); X-ray diffraction (Figure S3); EXAFS fitting results (Tables S1 and S2); probabilities of quadruple splitting and hyperfine internal magnetic field for Mössbauer spectra (Figure S4); and parameters of the spectra fits (Tables S3, S4) (PDF)

AUTHOR INFORMATION

Corresponding Author

Yuri L. Mikhlin − *Institute of Chemistry and Chemical Technology, Krasnoyarsk Science Center of the Siberian Branch of the Russian Academy of Sciences, Krasnoyarsk 660036, Russia;* ⓞ orcid.org/0000-0003-1801-0947; Email: yumikh@icct.ru

Authors

Maxim N. Likhatski − *Institute of Chemistry and Chemical Technology, Krasnoyarsk Science Center of the Siberian Branch of the Russian Academy of Sciences, Krasnoyarsk 660036, Russia*

Oleg A. Bayukov − *Kirensky Institute of Physics, Krasnoyarsk Science Center of the Siberian Branch of the Russian Academy of Sciences, Krasnoyarsk 660036, Russia*

Yuriy Knyazev − *Kirensky Institute of Physics, Krasnoyarsk Science Center of the Siberian Branch of the Russian Academy of Sciences, Krasnoyarsk 660036, Russia*

Dmitriy A. Velikanov − *Kirensky Institute of Physics, Krasnoyarsk Science Center of the Siberian Branch of the Russian Academy of Sciences, Krasnoyarsk 660036, Russia*

Yevgeny V. Tomashevich − *Institute of Chemistry and Chemical Technology, Krasnoyarsk Science Center of the Siberian Branch of the Russian Academy of Sciences, Krasnoyarsk 660036, Russia*

Alexander S. Romanchenko − *Institute of Chemistry and Chemical Technology, Krasnoyarsk Science Center of the Siberian Branch of the Russian Academy of Sciences, Krasnoyarsk 660036, Russia*

Sergey A. Vorobyev − *Institute of Chemistry and Chemical Technology, Krasnoyarsk Science Center of the Siberian Branch of the Russian Academy of Sciences, Krasnoyarsk 660036, Russia*

Mikhail V. Volochaev − *Kirensky Institute of Physics, Krasnoyarsk Science Center of the Siberian Branch of the Russian Academy of Sciences, Krasnoyarsk 660036, Russia;*

Reshetnev Siberian State University of Science and Technology, Krasnoyarsk 660037, Russia

Sergey M. Zharkov − Kirensky Institute of Physics, Krasnoyarsk Science Center of the Siberian Branch of the Russian Academy of Sciences, Krasnoyarsk 660036, Russia; Siberian Federal University, Krasnoyarsk 660041, Russia; orcid.org/0000-0002-3369-4112

Debora Motta Meira − European Synchrotron Radiation Facility, Grenoble F-38042, France

Complete contact information is available at:
https://pubs.acs.org/10.1021/acsomega.0c06052

Author Contributions

This manuscript was written through contributions of all authors. All authors have given approval to the final version of the manuscript.

Notes

The authors declare no competing financial interest.

■ REFERENCES

(1) Evans, H. T., Jr.; Allman, R. The Crystal Structure and Crystal Chemistry of Valleriite. *Z. Kristallogr.* **1968**, *127*, 73−93.

(2) Springer, G. Elecprobe analyses of macwite and valleriite. *Neues Jahrb. Mineral., Monatsh.* **1968**, *8*, 252−258.

(3) Hughes, A. E.; Kakos, G. A.; Turney, T. W.; Williams, T. B. Synthesis and Structure of Valleriite, a Layered Metal Hydroxide/Sulfide Composite. *J. Solid State Chem.* **1993**, *104*, 422−436.

(4) Li, R.; Cui, L. Investigations on Valleriite from Western China: Crystal Chemistry and Separation Properties. *Int. J. Miner. Process.* **1994**, *41*, 271−283.

(5) Qin, S.; Cao, Z.; Chen, Y. Preliminary Study on Crystal Chemistry of Valleriite. *Chin. Sci. Bull.* **1996**, *41*, 1982−1985.

(6) Chamberlain, J. A.; Delabio, R. N. Mackinawite and Valleriite in the Muskox Intrusion. *Am. Mineral.* **1965**, *50*, 682−695.

(7) Cabri, L. J. A New Copper-Iron Sulfide. *Econ. Geol.* **1967**, *62*, 910−925.

(8) Genkin, A. D.; Val'sov, L. N. O Valleriite i Machinovite i Uslovyakh ikh Nakhozhdeniya v Rudakh (On Valleriite and Makhinovite and Conditions of their Presence in Ores). *Geol. Rud. Mestorozhd.* **1967**, *9*, 94−106. (in Russian)

(9) Petruk, W.; Harris, D. C.; Murray, E. J. An Occurrence of Valleriite from New Imperial Mine, Yukon. *Can. Mineral.* **1971**, *10*, 885−888.

(10) Harris, D. C.; Vaughan, D. J. Two Fibrous Iron Sulfides and Valleriite from Cyprus with New Data on Valleriite. *Am. Mineral.* **1972**, *57*, 1037−1052.

(11) Mücke, A. Review on Mackinawite and Valleriite: Formulae, Localities, Associations and Intergrowths of the Minerals, Mode of Formation and Optical Features in Reflected Light. *J. Earth Sci. Clim. Change* **2017**, *8*, No. 1000419.

(12) Genkin, A. D.; Distler, V. V.; Gladyshev, G. D. *Sul'fidnye Medno-Nikelevye Rudy Noril'skikh Mestorozhdenii (Sulphidic Copper-Nickel Ores of Noril'sk Deposits)*; Nauka: Moscow, 1981; p 234, (in Russian).

(13) Dodin, D. A. *Metallogeniya Taimyro-Noril'skogo regiona (Metallogeny of Taimyr-Noril'sk region)*; Nauka: St.-Petersburg, 2002; p 374. (in Russian).

(14) Laptev, Y. V.; Shevchenko, V. S.; Urakaev, F. K. Sulphidation of Valleriite in SO_2 Solutions. *Hydrometallurgy* **2009**, *98*, 201−205.

(15) Burch, K. S.; Mandrus, D.; Park, J. Magnetism in Two-Dimensional van der Waals Materials. *Nature* **2018**, *563*, 47−52.

(16) Park, J.-G. Opportunities and Challenges of Two-Dimensional Magnetic van der Waals Materials: Magnetic Graphene? *J. Phys.: Condens. Matter* **2016**, *28*, No. 301001.

(17) Gao, T.; Zhang, Q.; Li, L.; Zhou, X.; Li, L.; Li, H.; Zhai, T. 2D Ternary Chalcogenides. *Adv. Opt. Mater.* **2018**, *6*, No. 1800058.

(18) Sethulakshmi, N.; Mishra, A.; Ajayan, P. M.; Kawazoe, Y.; Roy, A. K.; Singh, A. K.; Tiwary, C. S. Magnetism in Two-Dimensional Materials beyond Graphene. *Mater. Today* **2019**, *27*, 107−122.

(19) Cortie, D. L.; Causer, G. L.; Rule, K. C.; Fritzsche, H.; Kreuzpaintner, W.; Klose, F. Two-Dimensional Magnets: Forgotten History and Recent Progress towards Spintronic Applications. *Adv. Funct. Mater.* **2020**, *30*, No. 1901414.

(20) Du, Z.; Yang, S.; Li, S.; Lou, J.; Zhang, S.; Wang, S.; Li, B.; Gong, Y.; Song, L.; Zou, X.; Ajayan, P. M. Conversion of non-van der Waals Solids to 2D Transition-Metal Chalcogenides. *Nature* **2020**, *577*, 492−496.

(21) Verger, L.; Natu, V.; Carey, M.; Barsoum, M. W. MXenes: An Introduction of Their Synthesis, Select Properties, and Applications. *Trends Chem.* **2019**, *1*, 656−669.

(22) Li, Y.; Wang, Y.; Pattengale, B.; Yin, J.; An, L.; Cheng, F.; Li, Y.; Huang, J.; Xi, P. High-Index Faceted $CuFeS_2$ Nanosheets with Enhanced Behavior for Boosting Hydrogen Evolution Reaction. *Nanoscale* **2017**, *9*, 9230−9237.

(23) Ding, B. B.; Yu, C.; Li, C. X.; Deng, X. R.; Ding, J. X.; Cheng, Z. X.; Xing, B. G.; Ma, P.; Lin, J. *cis*-Platinum Pro-Drug-Attached $CuFeS_2$ Nanoplates for in vivo Photothermal/Photoacoustic Imaging and Chemotherapy/Photothermal Therapy of Cancer. *Nanoscale* **2017**, *9*, 16937−16949.

(24) Zhou, X.; Eckberg, C.; Wilfong, B.; Liou, S.-C.; Vivanco, H. K.; Paglione, J.; Rodriguez, E. E. Superconductivity and Magnetism in Iron Sulfides Intercalated by Metal Hydroxides. *Chem. Sci.* **2017**, *8*, 3781−3788.

(25) Agamah, C.; Vuori, S.; Colinet, P.; Norrbo, I.; de Carvalho, J. M.; Nakamura, L. K. O.; Lindblom, J.; van Goethem, L.; Emmermann, A.; Saarinen, T.; Laihinen, T.; Laakkonen, E.; Lindén, J.; Konu, J.; Vrielinck, H.; Van der Heggen, D.; Smet, P. F.; Bahers, T. L.; Lastusaari, M. Hackmanite—The Natural Glow-in-the-Dark Material. *Chem. Mater.* **2020**, *32*, 8895−8905.

(26) O'Connor, D.; Hou, D.; Liu, Q.; Palmer, M. R.; Varma, R. S. Nature-Inspired and Sustainable Synthesis of Sulfur-Bearing Fe-Rich Nanoparticles. *ACS Sustainable Chem. Eng.* **2020**, *8*, 15791−15808.

(27) Harris, D. C.; Cabri, L. J.; Stewart, J. M. A "Valleriite-Type" Mineral from Noril'sk, Western Siberia. *Am. Mineral.* **1970**, *55*, 2110−2114.

(28) Emelina, L. N.; Mitenkov, G. A.; Karchenkov, A. M. In *Chemical Composition of Valleriite. Zapiski VMO*, Proceedings of the Russian Mineralogical Society; 1982; pp 84−92. (in Russian)

(29) Iishi, K.; Tomisaka, T.; Kato, T.; Takeno, S. Syntheses of Valleriite. *Am. Mineral.* **1970**, *55*, 2107−2110.

(30) Waanders, F. B.; Pollak, H. Mössbauer Spectroscopy to Characterize Iron Sulphides. *S. Afr. J. Sci.* **1999**, *95*, 387−390.

(31) Mikhlin, Y. L.; Romanchenko, A. S.; Tomashevich, E. V.; Volochaev, M. N.; Laptev, YuV. XPS and XANES Study of Layered Mineral Valleriite. *J. Struct. Chem.* **2017**, *58*, 1137−1143.

(32) Chistyakova, N. I.; Gubaidulina, T. V.; Rusakov, V. S. Mossbauer Investigations of Natural and Synthetic Tochilinite and Valleriite. *Czech. J. Phys.* **2006**, *56*, 123−E131.

(33) Gubaidulina, T. V.; Chistyakova, N. I.; Rusakov, V. S. Mössbauer Study of Layered Iron Hydroxysulfides: Tochilinite and Valleriite. *Bull. Russ. Acad. Sci. Phys.* **2007**, *71*, 1269−1272.

(34) Chistyakova, N. I.; Rusakov, V. S.; Gubaidulina, T. V.; Gapochka, A. M.; Bychkov, A. Yu. Mössbauer Investigations of Synthetic Valleriite. *Hyperfine Interact.* **2012**, *208*, 99−104.

(35) Mikhlin, Y.; Romanchenko, A.; Vorobyev, S.; Karasev, S.; Volochaev, M.; Kamenskiy, E.; Burdakova, E. Ultrafine Particles in

Ground Sulfide Ores: A Comparison of Four Cu–Ni Ores from Siberia, Russia. *Ore Geol. Rev.* **2017**, *81*, 1−9.

(36) Mikhlin, Y.; Tomashevich, Y.; Tauson, V.; Vyalikh, D.; Molodtsov, S.; Szargan, R. A Comparative X-ray Absorption Near-Edge Structure Study of Bornite, Cu_5FeS_4, and Chalcopyrite, $CuFeS_2$. *J. Electron Spectrosc. Relat. Phenom.* **2005**, *142*, 85−90.

(37) Mikhlin, Y.; Nasluzov, V.; Romanchenko, A.; Tomashevich, Y.; Shor, A.; Félix, R. Layered Structure of the Near-Surface Region of Oxidized Chalcopyrite ($CuFeS_2$): Hard X-Ray Photoelectron Spectroscopy, X-Ray Absorption Spectroscopy and DFT+U Studies. *Phys. Chem. Chem. Phys.* **2017**, *19*, 2749−2759.

(38) Nasluzov, V.; Shor, A.; Romanchenko, A.; Tomashevich, Y.; Mikhlin, Y. DFT+U and Low-Temperature XPS Studies of Fe-Depleted Chalcopyrite ($CuFeS_2$) Surfaces: A Focus on Polysulfide Species. *J. Phys. Chem. C* **2019**, *123*, 21031−21041.

(39) Mathon, O.; Beteva, A.; Borrel, J.; Bugnazet, D.; Gatla, S.; Hino, R.; Kantor, I.; Mairs, T.; Munoz, M.; Pasternak, S.; Perrin, F.; Pascarelli, S. The Time-Resolved and Extreme Conditions XAS (TEXAS) Facility at the European Synchrotron Radiation Facility: The General-Purpose EXAFS Bending-Magnet Beamline BM23. *J. Synchrotron Radiat.* **2015**, *22*, 1548−1554.

(40) Ravel, B.; Newville, M. ATHENA, ARTEMIS, HEPHAESTUS: Data Analysis for X-Ray Absorption Spectroscopy Using IFEFFIT. *J. Synchrotron Radiat.* **2005**, *12*, 537−541.

(41) Bataleva, Y.; Palyanov, Y.; Borzdov, Y.; Bayukov, O. Processes and Conditions of the Origin for Fe^{3+}-Bearing Magnesiowüstite under Lithospheric Mantle Pressures and Temperatures. *Minerals* **2019**, *9*, 474.

(42) Sazonov, A. M.; Silyanov, S. A.; Bayukov, O. A.; Knyazev, Y. V.; Zvyagina, Y. A.; Tishin, P. A. Composition and Ligand Microstructure of Arsenopyrite from Gold Ore Deposits of the Yenisei Ridge (Eastern Siberia, Russia). *Minerals* **2019**, *9*, 737.

(43) Velikanov, D. A. High-Sensitivity Measurements of the Magnetic Properties of Materials at Cryogenic Temperatures. *Inorg. Mater. Appl. Res.* **2020**, *11*, 801−808.

(44) Velikanov, DA. Vibration Magnetic Meter. RF patent for the invention RU2341810 (C1).Publ. 20.12.2008, Bull. No. 35. http://www.freepatent.ru/patents/2341810.

(45) Waychunas, G. A.; Apted, M. J.; Brown, G. E., Jr. X-Ray K-Edge Absorption Spectra of Fe Minerals and Model Compounds: Near-Edge Structure. *Phys. Chem. Minerals* **1983**, *10*, 1−9.

(46) Wilke, M.; Farges, F.; Petit, P.-E.; Brown, G. E., Jr; Martin, F. Oxidation State and Coordination of Fe in Minerals: An Fe K-XANES Spectroscopic Study. *Am. Mineral.* **2001**, *86*, 714−730.

(47) Baker, M. L.; Mara, M. W.; Yan, J. M.; Hodgson, K. O.; Hedman, B.; Solomon, E. I. K- and L-Edge X-Ray Absorption Spectroscopy (XAS) and Resonant Inelastic X-Ray Scattering (RIXS) Determination of Differential Orbital Covalency (DOC) of Transition Metal Sites. *Coord. Chem. Rev.* **2017**, *345*, 182−208207.

(48) Sutton, S. R.; Lanzirotti, A.; Newville, M.; Darby Dyar, M.; Delaney, J. Oxybarometry and Valence Quantification Based on Microscale X-Ray Absorption Fine Structure (XAFS) Spectroscopy of Multivalent Elements. *Chem. Geol.* **2020**, *531*, No. 119305.

(49) Petiau, J.; Sainctavit, P.; Calas, G. K X-Ray Absorption Spectra and Electronic Structure of Chalcopyrite $CuFeS_2$. *Mater. Sci. Eng. B* **1988**, *1*, 237−249.

(50) England, K. E. R.; Charnock, J. M.; Pattrick, R. A. D.; Vaughan, D. J. Surface Oxidation Studies of Chalcopyrite and Pyrite by Glancing-Angle X-ray Absorption Spectroscopy (REFLEXAFS). *Mineral. Mag.* **1999**, *63*, 559−566.

(51) Šipr, O.; Machek, P.; Šimůnek, A. Cu, Fe, and S K- and L-Edge XANES Spectra of $CuFeS_2$: Localization and Interpretation of Pre-Peak States. *Phys. Rev. B* **2004**, *69*, No. 155115.

(52) De Lima, G. F.; Duarte, H. A.; Pettersson, L. G. M. X-ray Absorption Near-Edge Spectroscopy Calculations on Pristine and Modified Chalcopyrite Surfaces. *J. Phys. Chem. C* **2018**, *122*, 20200−20209.

(53) Martinelli, A.; Orazio Lepore, G.; Bernardini, F.; Giaccherini, A.; Di Benedetto, F. The Puzzling Structure of Cu_5FeS_4 (Bornite) at Low Temperature. *Acta Crystallogr., Sect. B: Struct. Sci., Cryst. Eng. Mater.* **2018**, *74*, 405−415.

(54) Borgheresi, M.; Di Benedetto, F.; Romanelli, M.; Reissner, M.; Lottermoser, W.; Gainov, R. R.; Khassanov, R. R.; Tippelt, G.; Giaccherini, A.; Sorace, L.; Montegrossi, G.; Wagner, R.; Amthauer, G. Mössbauer Study of Bornite and Chemical Bonding in Fe-Bearing Sulphides. *Phys. Chem. Minerals* **2018**, *45*, 227−235.

(55) Li, D.; Bancroft, G. M.; Kasrai, M.; Fleet, M. E.; Feng, X. H.; Yang, B. X.; Tan, K. H. S K- and L-Edge XANES and Electronic Structure of Some Copper Sulfide Minerals. *Phys. Chem. Minerals* **1994**, *21*, 317−324.

(56) Goh, S. W.; Buckley, A. N.; Lamb, R. N.; Rosenberg, R. A.; Moran, D. The Oxidation States of Copper and Iron in Mineral Sulfides, and the Oxides Formed on Initial Exposure of Chalcopyrite and Bornite to Air. *Geochim. Cosmochim. Acta* **2006**, *70*, 2210−2228.

(57) Grosvenor, A. P.; Kobe, B. A.; Biesinger, M. C.; McIntyre, N. S. Investigation of Multiplet Splitting of Fe 2p XPS Spectra and Bonding in Iron Compounds. *Surf. Interface Anal.* **2004**, *36*, 1564−1574.

(58) Marfunin, A. S.; Mkrtchyan, A. R. Mössbauer Spectra of Fe^{57} in Sulfides. *Geochem. Int.* **1967**, *4*, 980−989.

(59) Marusak, L. A.; Mulay, L. N. Mössbauer and Magnetic Study of the Antiferro to Ferrimagnetic Phase Transition in Fe_9S_{10} and the Magnetokinetics of the Diffusion of Iron Atoms during the Transition. *J. Appl. Phys.* **1979**, *50*, 1865−1867.

(60) Jeandey, C.; Oddou, J. L.; Mattei, J. L.; Fillion, G. Mössbauer Investigation of the Pyrrhotite at Low Temperature. *Solid State Commun.* **1991**, *78*, 195−198.

(61) Kondoro, J. W. A.; Kiwanga, C. A. Moessbauer Study of Natural Pyrrhotites. *Appl. Radiat. Isot.* **1997**, *48*, 555−563.

(62) Kondoro, J. Mössbauer Study of Natural Iron-Oxide Complexes. *Hyperfine Interact.* **1999**, *120*, 535−538.

(63) *Mössbauer Mineral Handbook*; Stevens, J. G.; Khasanov, A. M.; Miller, J. W.; Pollak, H.; Li, Z., Eds.; Mössbauer Effect Data Center: Asheville, North Carolina, 2005.

(64) Vandenberghe, R. E.; De Grave, E. Application of Mössbauer Spectroscopy in Earth Sciences. In *Mössbauer Spectroscopy*;Yoshida, Y.; Langouche, G., Eds.; Springer: Berlin, Heidelberg, 2013; pp 91−185.

(65) Aramu, F.; Bressani, T.; Manca, P. *On the Mössbauer effect of chalcopyrite* **1967**, *51*, 370−375.

(66) Boekema, C.; Krupski, A. M.; Varasteh, M.; Parvin, K.; van Til, F.; van der Woude, F.; Sawatzky, G. A. Cu and Fe Valence States in $CuFeS_2$. *J. Magn. Magn. Mater.* **2004**, *272−276*, 559−561.

(67) Mussel, W. N.; Murad, E.; Fabris, J. D.; Moreira, W. S.; Barbosa, J. B. S.; Murta, C. C.; Abrahão, W. P.; De Mello, J. W. V.; Garg, V. K. Characterization of a Chalcopyrite from Brazil by Mössbauer Spectroscopy and Other Physicochemical Techniques. *Phys. Chem. Minerals* **2007**, *34*, 383−387.

(68) Oddou, J. L.; Jeandey, C.; Mattei, J. L.; Fillion, G. Mössbauer Study of the Low-Temperature Transition in Pyrrhotite. *J. Magn. Magn. Mat.* **1992**, *104−107*, 1987−1988.

(69) Wolfers, P.; Fillion, G.; Ouladdiaf, B.; Ballou, R.; Rochette, P. The Pyrrhotite 32K Magnetic Transition. *Solid State Phenom.* **2011**, *170*, 174−179.

(70) Haines, C. R. S.; Dutton, S. E.; Volk, M. W. R.; Carpenter, M. A. Magnetoelastic Properties and Behaviour of 4C Pyrrhotite, Fe_7S_8, through the Besnus Transition. *J. Phys.: Condens. Matter* **2020**, *32*, No. 405401.

(71) Dorogina, G. A.; Titova, S. G.; Gulyaeva, R. I.; Selivanov, E. N. Magnetic Properties of Pyrrhotine with the Hexagonal Structure in the Temperature Range of 4−300 K. *Phys. Solid State* **2015**, *57*, 689−693.

(72) Rais, A.; Gismelseed, A. M.; Al-Rawas, A. D. Magnetic Properties of Natural Chalcopyrite at Low Temperature. *Mater. Lett.* **2000**, *46*, 349−353.

(73) Conejeros, S.; Alemany, P.; Llunell, M.; Moreira, I. d. P. R.; Sánchez, V.; Llanos, J. Electronic Structure and Magnetic Properties of $CuFeS_2$. *Inorg. Chem.* **2015**, *54*, 4840−4849.

(74) Navrátil, J.; Levinský, P.; Hejtmánek, J.; Pashchenko, M.; Knížek, K.; Kubícková, L.; Kmjec, T.; Drašar, C. Peculiar Magnetic and Transport Properties of $CuFeS_2$: Defects Play a Key Role. *J. Phys. Chem. C* **2020**, *124*, 20773−20783.

(75) Richter, C.; van der Pluijm, B. A. Separation of Paramagnetic and Ferrimagnetic Susceptibilities using Low Temperature Magnetic Susceptibilities and Comparison with High Field Methods. *Phys. Earth Planet. Inter.* **1994**, *83*, 113−123.

(76) Martín-Hernández, F.; Ferré, E. C. Separation of Paramagnetic and Ferrimagnetic Anisotropies: A Review. *J. Geophys. Res.* **2007**, *112*, No. B03105.

(77) Rogozin, D. Y.; Balaev, D. A.; Semenov, S. V.; Shaikhutdinov, K. A.; Bayukov, O. A. Magnetic Properties of Bottom Sediments from Meromectic Shira Lake (Siberia, Russia). *Dokl. Earth Sc.* **2016**, *469*, 819−823.

(78) Peddis, D.; Rinaldi, D.; Ennas, G.; Scano, A.; Agostinelli, E.; Fiorani, D. Superparamagnetic Blocking and Superspin-Glass Freezing in Ultra Small δ-$(Fe_{0.67}Mn_{0.33})OOH$ Particles. *Phys. Chem. Chem. Phys.* **2012**, *14*, 3162−3169.

(79) Dormann, J. L.; Cherkaoui, R.; Spinu, L.; Noguès, M.; Lucari, F.; D'Orazio, F.; Fiorani, D.; Garcia, A.; Tronc, E.; Jovilet, J. P. From Pure Superparamagnetic Regime to Glass Collective State of Magnetic Moments in γ-Fe_2O_3 Nanoparticle Assemblies. *J. Magn. Magn. Mater.* **1998**, *187*, L139−L144.

(80) López de la Torre, M. A.; Peña, V.; Sefrioui, Z.; Arias, D.; Leon, C.; Santamaria, J.; Martinez, J. L. Paramagnetic Meissner Effect in $YBa_2Cu_3O_7$/$La_{0.7}Ca_{0.3}MnO_3$ Superlattices. *Phys. Rev. B* **2006**, *73*, No. 052503.

(81) Popkov, S. I.; Krasikov, A. A.; Semenov, S. V.; Dubrovskii, A. A.; Yakushkin, S. S.; Kirillov, V. L.; Mart'yanov, O. N.; Balaev, D. A. Features of the Pulsed Magnetization Switching in a High-Coercivity Material Based on ε-Fe_2O_3 Nanoparticles. *Phys. Solid State* **2020**, *62*, 445−453.

(82) Borgheresi, M.; Di Benedetto, F.; Caneschi, A.; Pratesi, G.; Romanelli, M.; Sorace, L. An EPR and SQUID Magnetometry Study of Bornite. *Phys. Chem. Minerals* **2007**, *34*, 609−619.

(83) Gainov, R. R.; Vagizov, F. G.; Golovanevskiy, V. A.; Ksenofontov, V. A.; Klingelhöfer, G.; Klekovkina, V. V.; Shumilova, T. G.; Pen'kov, I. N. Application of ^{57}Fe Mössbauer Spectroscopy as a Tool for Mining Exploration of Bornite (Cu_5FeS_4) Copper Ore. *Hyperfine Interact.* **2014**, *226*, 51−55.

(84) Mikhlin, Y. L.; Tomashevich, Y. V.; Asanov, I. P.; Okotrub, A. V.; Varnek, V. A.; Vyalikh, D. V. Spectroscopic and Electrochemical Characterization of the Surface Layers of Chalcopyrite $(CuFeS_2)$ Reacted in Acidic Solutions. *Appl. Surf. Sci.* **2004**, *225*, 395−409.

(85) Lyubutin, I. S.; Lin, C.-R.; Starchikov, S. S.; Siao, Y.-J.; Shaikh, M. O.; Funtov, K. O.; Wang, S.-C. Synthesis, Structural and Magnetic Properties of Self-Organized Single-Crystalline Nanobricks of Chalcopyrite $CuFeS_2$. *Acta Mater.* **2013**, *61*, 3956−3962.

(86) Zhang, Y.; Zhao, G.; Xin Lv, X.; Tian, Y.; Yang, L.; Zou, G.; Hou, H.; Zhao, H.; Ji, X. Exploration and Size Engineering from Natural Chalcopyrite to High-Performance Electrode Materials for Lithium-Ion Batteries. *ACS Appl. Mater. Interfaces* **2019**, *11*, 6154−6165.

(87) Pekov, I. V.; Sereda, E. V.; Yapaskurt, V. O.; Polekhovsky, Y. S.; Britvin, S. N.; Chukanov, N. V. Ferrovalleriite, $2(Fe,Cu)S \cdot 1.5Fe(OH)_2$: Validation as a Mineral Species and New Data. *Geol. Ore Deposits* **2013**, *55*, 637−647.

(88) Nickel, E. H.; Hudson, D. R. The Replacement of Chrome Spinel by Chromian Valleriite in Sulphide-Bearing Ultramafic Rocks in Western Australia. *Contrib. Mineral. Petrol.* **1976**, *55*, 265−277.

(89) Starchikov, S. S.; Lyubutin, I. S.; Lin, C.-R.; Tseng, Y.-T.; Funtov, K. O.; Ogarkova, YuL.; Dmitrieva, T. V.; Ivanova, A. G. Synthesis and Magnetic Properties of the Chromium-Doped Iron Sulfide $Fe_{1-x}Cr_xS$ Single Crystalline Nanoplates with a NiAs Crystal Structure. *Phys. Chem. Chem. Phys.* **2015**, *17*, 15829−15836.

(90) Barber, D.; Bourdillon, A.; Freeman, L. Fe-Ni-S-O Layer Phase in C2M Carbonaceous Chondrites—a Hydrous Sulphide? *Nature* **1983**, *305*, 295−297.

(91) Organova, N. I. *Kristallokhimiya Nesorazmernykh i Modulirovannykh Smeshannosloinykh Mineralov(Crystal Chemistry of Incomensurate and Modulated Mixed-Layer Minerals)* Nauka: Moscow, 1989. (In Russian).

(92) Pekov, I. V.; Sereda, E. V.; Polekhovsky, Y. S.; Britvin, S. N.; Chukanov, N. V.; Yapaskurt, V. O.; Bryzgalov, I. A. Ferrotochilinite, $6FeS \cdot 5Fe(OH)_2$, a New Mineral from the Oktyabr'sky Deposit, Noril'sk District, Siberia, Russia. *Geol. Ore Deposits* **2013**, *55*, 567−574.